**7676** *Inorg. Chem.* **2010**, *49*, 7676–7684
DOI: 10.1021/ic100024h

Inorganic Chemistry
Article

# Torsionally Controlled Electronic Coupling in Mixed-Valence Oxodimolybdenum Nitrosyl Scorpionates - a DFT Study

**Piotr P. Romańczyk,*,† Klemens Noga,‡ Andrzej J. Włodarczyk,† Wojciech Nitek,‡ and Ewa Broclawik*,§**

†*Faculty of Chemical Engineering and Technology, Cracow University of Technology, ul. Warszawska 24, 31-155 Kraków, Poland* , ‡*Faculty of Chemistry, Jagiellonian University, Ingardena 3, 30-060 Kraków, Poland* , and §*Institute of Catalysis and Surface Chemistry, Polish Academy of Sciences, ul. Niezapominajek 8, 30-239 Kraków, Poland*

Received January 5, 2010

The density functional theory (DFT) method has been used to study the electronic communication in strongly interacting oxo-bridged di-$\{Mo^{II,I}(NO^{+})\}^{3+,2+}$ complexes stabilized by tris(3-methylpyrazol-1-yl)borate, $[Tp^{Me}]^{-}$ (dihydroxy **1′** and its modified analogs), having fully localized valences on the two Mo centers (Class I), despite a short (ca. 3.8 Å) Mo···Mo distance. Structural and electrochemical (separation between the redox potentials $\Delta_{red/ox}E_{1/2}$) properties and IR spectra (in particular the $\nu_{NO}$ frequencies) obtained from the B3LYP calculations for **1′** are successfully related to experimental values. Strongly twisted geometry with the (O)N−Mo1···Mo2−N(O) angle close to 90° (confirmed by DFT modeling performed for $\mathbf{1'}^{-1,0,+1}$ and X-ray diffraction study of $[\{Mo(NO)(Tp^{Me2})(OH)\}_2(\mu\text{-}O)]^{-}$ (**1**) presented herein) is a common, though so far not fully understood, structural feature of this class of $\mu$-oxo species, in contrast to the closely related $\{Mo^{V}(=O)\}^{3+}$ analogs. This study shows that the orthogonality of the local equatorial planes for the two Mo centers may be rationalized by the electronic structure, namely from the balance between the destabilizing repulsion of the Mo-based $(d, \pi_x^*)_b$ electron pairs versus a favorable but relatively weak electron delocalization. Strongly repelling electron pairs avoid each other, which enforces the twisted geometries and blocks the electron delocalization. Steric hindrance (a nonbonding repulsion of the adjacent $Tp^{x}$ ligands and the weak hydrogen-bonding interactions, i.e., OH···ON, OH···OH, and C−H···$O_{(NO/OH)}$) is shown not to be decisive since neither the removal of the inner 3-Me groups of $[Tp^{Me}]^{-}$ in complex **1′** nor the substitution of OH groups by $OCH_3$ ligands did substantially influence the dihedral twist angle in the minimum energy structure. Yet the relative orientation of the $\{Mo(NO)\}^{2+,3+}$ cores along with the position of the bridging oxygen (significantly bent upon reduction) controls the prospective intramolecular through-bond electron transfer in the mixed valence form. Our DFT modeling demonstrates that a maximum delocalization (via a hole-transfer mechanism) of the unpaired electron in $\mathbf{1'}^{-}$, measured as a spin population on the nonreduced Mo2 center, is achieved for the structure with a torsional deflection of 23°, at a cost of 16.5 kcal/mol. These results show that the electron exchange along the Mo−O−Mo array in the originally fully valence-trapped $\{17e{:}16e\}^{-}$ complexes may be controlled and can be thermally activated (e.g., using a high-boiling solvent or by irradiation at ca. 50−200 $cm^{-1}$).

## Introduction

Mixed-valence bi- and oligometallic complexes based on $\{Mo^{II-0}(NO^{+})\}^{3+,2+,1+}$ and on the closely related $\{Mo^{VI-IV}(=O)\}^{4+,3+,2+}$ cores stabilized by hydrotris(3,5-dimethylpyrazol-1-yl)borate, $[Tp^{Me2}]^{-}$, depending on the nature of the bridging ligand, demonstrate astonishing electronic and magnetic properties which could be useful in designing new molecular materials and devices.[1−3] Despite the fact that $\{Mo(O)Tp^{x}\}$ species were used in enzyme modeling a long time ago,[4] only recently it has been shown that $\{Mo(NO)(Tp^{Me2})\}$ complexes, having an easily tunable redox potential, efficiently catalyze the cathodic reduction of chloroform.[5,6] The bimetallic $[X(Tp^{Me2})(ON)MoOMo(NO)(Tp^{Me2})Y]^{-}$ (X, Y = anionic coligands like halide, alkoxide, hydroxide, and carboxylate)[7,8] complexes

*Corresponding author. E-mail: broclawi@chemia.uj.edu.pl.

(1) McCleverty, J. A.; Ward, M. D. *Acc. Chem. Res.* **1998**, *31*, 842.
(2) McCleverty, J. A.; Ward, M. D.; Jones, C. J. *Comments Inorg. Chem.* **2001**, *22*, 293.
(3) Ward, M. D.; McCleverty, J. A. *J. Chem. Soc., Dalton Trans.* **2002**, 275.
(4) Enemark, J. H.; Cooney, J. J. A.; Wang, J.-J.; Holm, R. H. *Chem. Rev.* **2004**, *104*, 1175.
(5) Włodarczyk, A. J.; Romańczyk, P. P.; Lubera, T.; Kurek, S. S. *Electrochem. Commun.* **2008**, *10*, 1856.
(6) Włodarczyk, A. J.; Romańczyk, P. P. *Inorg. Chim. Acta* **2009**, *362*, 4635.
(7) Wlodarczyk, A.; Maher, J. P.; Coles, S.; Hibbs, D. E.; Hursthouse, M. H. B.; Malik, K. M. A. *J. Chem. Soc., Dalton Trans.* **1997**, 2597.
(8) Wlodarczyk, A.; Coles, S. J.; Hursthouse, M. B.; Abdul, K. M.; Lieberman, H. F. *J. Chem. Soc., Dalton Trans.* **1997**, 2921.

 Published on Web 07/27/2010 

together with the Creutz−Taube analogue[9] [{Mo(NO)-(Tp$^{Me2}$)Br}$_2$($\mu$-pz)]$^-$ (both $S = 1/2$) are among the strongest interacting mixed-valence systems known. Huge electrochemical interactions in the latter case ($\Delta E_{1/2}$ = 1440 mV, in $CH_2Cl_2$) go hand in hand with an effectively delocalized extra electron over the Mo centers and the 6.9 Å pyrazine bridge in the {17*e*:18*e*}$^-$ state on both electron paramagnetic resonance (EPR, ca. $10^{-8}$ s) and IR (ca. $10^{-13}$ s) time-scales (class III in the Robin−Day classification scheme).

The great separation between two one-electron reductions ($\Delta E_{1/2}$ > 1000 mV, in $CH_2Cl_2$) recorded for the oxo-bridged complexes of {Mo(NO)(Tp$^{Me2}$)X}$^+$ arises, however, not from the through-bond effects but from the through-space metal−metal interactions in the {17*e*:16*e*}$^-$ state, i.e., a change in electron density on one Mo center is communicated to the other by Coulombic interactions. A common feature of these $\mu$-oxo compounds, besides a large redox potential splitting, is the hyperfine coupling ($A_{Mo}$) close to 50 G and the two $\nu_{NO}$ bands (shifted to red with respect to those for precursors) consistent with a single-electron coupled to a Mo nucleus (Class I at room temperature, r.t.), which is in accordance with the appearance of very weakly solvatochromic absorption bands[10] in the near-IR region. These entirely valence-trapped systems are rare and unexpected examples among the symmetrically substituted oxo-bridged bimetallics[11] (Mo···Mo distance ca. 3.8 Å) having a doublet ground state (which does not originate from a large antiferromagnetic coupling),[12] and their properties could be explained by the structural relationship of the {Mo(NO)-(Tp$^{Me2}$)} fragments. In the class of compounds studied here, with either symmetrically (X = Y) or asymmetrically (X ≠ Y) substituted centers, X-ray diffraction shows the nitrosyl ligands (assumed being on the local *z* axis) actually lying along perpendicular directions. Thus, the redox Mo $d_{xy}$ orbitals are mutually orthogonal and cannot overlap via the oxygen p orbitals, hence the metal configuration is $(d_{xy})^1-O-(d_{xy})^0$, as confirmed by our density functional theory (DFT) calculations. Additionally, the Mo−O−Mo bond angle is significantly smaller than 180° (av. 171°) as a result of the interligand steric interactions. However, the temperature dependent EPR spectra of benzoate or chloride {(ON)MoOMo(NO)}$^{3+}$ complexes belonging to the class addressed in this study suggest that the electron exchange across the Mo−O−Mo array could also start with a temperature increase,[8] triggering a prospective rotational freedom.

Those properties described above can be contrasted with the behavior of [{LMo$^{V,VI}$O$_2$}$_2$($\mu$-O)]$^+$ (L is *N*,*N*′,*N*″-trimethyl-1,4,7-triazacyclononane)[13] and [{Ru$^{III,IV}$(NH$_3$)$_5$}$_2$-($\mu$-O)]$^{5+}$ complexes,[14] which appear to be delocalized on the basis of the EPR/IR or electron spectroscopy for chemical analysis (ESCA) data. Another example of a delocalized system is the structurally characterized [{(HCO$_2$)(NH$_3$)$_4$-Ru}$_2$($\mu$-O)]$^{3+}$ containing a nearly linear Ru$^{III}$−O−Ru$^{IV}$ system with both metals in identical coordination environments.[15] A greater degree of mixing between the $d_\pi$ orbitals at metals with two p orbitals at the bridging oxygen and, consequently, an electronic delocalization, was suggested to result in the lowering of the structural asymmetry in the metal−oxygen distances in [{(tpy)(bpy)Os$^{III,IV}$}$_2$($\mu$-O)]$^{5+}$ (tpy is 2,2′:6′,2″-terpyridine and bpy is 2,2′-bipyridine) when compared to [{(bpy)$_2$ClRu$^{III,IV}$}$_2$($\mu$-O)]$^{3+}$.[16] Furthermore, the linear ON−Ru−O−Ru−NO arrangement in the [{Ru$^{II}$-Cl$_2$(NO)(dmpH)$_2$}$_2$($\mu$-O)] (dmpH is 3,5-dimethylpyrazole) points to a delocalized $\pi$-bonding model,[17] which should also be operating in a mixed-valence state. Suitable examples can also be found for the first-row transition metals. Delocalization of the unpaired electron was evidenced by spectroscopic, electrochemical, and X-ray studies performed for the oxo-bridged vanadium complexes containing a tripodal *tris*[benzimidazol-2′-yl-methyl]amine or its Me-analog, [{(R$_3$ntb)-VO}$_2$($\mu$-O)]$^{3+}$ (R = H or Me).[18] Similarly, the extensive extra electron delocalization in [{VO(HOsal-Gly)}$_2$($\mu$-O)]$^-$ (HOsal-Gly is 4-hydroxysalicylideneglycinate) was confirmed by DFT calculations,[19] despite a small asymmetry of the $V^{IV}-O-V^V$ bridge.

In this study we present DFT calculations of the electronic structure of a neutral form along with a mixed-valence monoanion and a monocation derived from the previously reported[8] [(HO)(Tp$^{Me2}$)(ON)MoOMo(NO)(Tp$^{Me2}$)(OH)] (**1**) complex. Crystal structure of **1** has also been determined. The main objective of this study was to characterize factors affecting the degree of conceivable through-bond electronic coupling between the metal-based centers in the originally fully localized interlocking system. One such factor is the relative orientation of the {Mo(NO)}$^{2+/3+}$ groups. The rotational freedom of a bridging unit (changing the relative orientation of the NO groups) may be the source of rheostat properties.[20] The effect of prospective steric hindrance on the geometry and electronic properties was studied by removing the inner 3-methyl groups in the pyrazolyl rings as well as by a substitution of the hydroxy by the methoxy ligands. These effects were found insignificant. On the other hand, based on the obtained electronic structure, we proposed that the

(9) Wlodarczyk, A.; Doyle, G. A.; Maher, J. P.; McCleverty, J. A.; Ward, M. D. *Chem. Commun.* **1997**, 769.

(10) McWhinnie, S. L. W.; Charsley, S. M.; Jones, C. J.; McCleverty, J. A.; Yellowlees, L. J. *J. Chem. Soc., Dalton Trans.* **1993**, 413.

(11) It should be noted here that there exists rare fully valence-trapped oxo-bridged $V^{IV}/V^V$ bimetallics (Class I, both in the solid and in solution) but with the other reason for stabilization of localized electronic structure. The $\pi$-donor ability of the equatorial ligands, i.e., the d$\pi$(V)−p$\pi$(O$_{phenolate}$) interactions are claimed stronger for $V^V$ than $V^{IV}$ center (e.g., the structurally characterized complex with identically coordinated vanadium(IV/V) centers, [L$_2$V$_2$O$_3$](ClO$_4$)·0.5acetone (L is deprotonated *N*-(2-hydroxybenzyl)-1,4,7-triazacyclononane), with the torsion angle O$_t$V···VO$_t$ of 176.5°, see: Schulz, D.; Weyhermüller, T.; Wieghardt, K.; Nuber, B. *Inorg. Chim. Acta* **1995**, *240*, 217.

(12) As for example in the Mn(III)−O−Mn(IV) system with strongly antiferromagnetically coupled centers, see Horner, O. *Inorg. Chem.* **1999**, *38*, 1222. In [(bpy)$_2$(OH$_x$)RuORu(OH$_y$)(bpy)$_2$]$^{z+}$ complexes, the AF coupled states are preferred than electron delocalization over RuORu (see Yang, X.; Baik, M.-H. *J. Am. Chem. Soc.* **2004**, *126*, 13222.

(13) Wieghardt, K.; Backes-Dahmann, G.; Herrmann, W.; Weiss, J. *Angew. Chem., Int. Ed. Engl.* **1984**, *23*, 899. Herrmann, W.; Wieghardt, K. *Polyhedron* **1986**, *5*, 513.

(14) Baumann, J. A.; Meyer, T. J. *Inorg. Chem.* **1980**, *19*, 345.

(15) Emerson, J.; Clarke, M. J.; Ying, W.-L.; Sanadi, D. R. *J. Am. Chem. Soc.* **1993**, *115*, 11799.

(16) Schoonover, J. R.; Ni, J.; Roecker, L.; White, P. S.; Meyer, T. J. *Inorg. Chem.* **1996**, *35*, 5885.

(17) Bohle, D. S.; Sagan, E. S. *Eur. J. Inorg. Chem.* **2000**, 1609.

(18) Ghosh, S.; Nanda, K. K.; Addison, A. W.; Butcher, R. J. *Inorg. Chem.* **2002**, *41*, 2243.

(19) Costa Pessoa, J.; Calhorda, M. J.; Cavaco, I.; Correia, I.; Duarte, M. T.; Felix, V.; Henriques, R. T.; Piedade, M. F. M.; Tomaz, I. *J. Chem. Soc., Dalton Trans.* **2002**, 4407.

(20) We were inspired at this point by studies performed in the Chisholm group which examined electronic factors associated with M$_2$ (M = Mo or W) unit linked by functionalized terephthalate bridges (see Chisholm, M. H.; Feil, F.; Hadad, C. M.; Patmore, N. J. *J. Am. Chem. Soc.* **2005**, *127*, 18150.

repulsion between the electron pairs in the $d_{xz}$ orbitals on two Mo centers might highly influence relative orientation of NO ligands, pushing them apart. Moreover, voltammetrically established potentials of formation of both $\{17e{:}16e\}^-$ and $\{16e{:}15e\}^+$ complexes together with the IR spectra (especially the $\nu_{NO}$ and $\nu_{MoOMo}$ frequencies) and the crystal data of the precursor complex have been successfully related to the computed parameters which additionally validated our model.

## Experimental Section

**Computational Details. Models.** All computational results reported in this paper were obtained on a mimetic model of complex **1** (called here **1′**) and its reduced/oxidized forms ($\mathbf{1'}^z$, $z = 2-,1-,1+$, and $2+$), where the outer methyl groups of $[Tp^{Me2}]^-$ ligand were cut off to minimize an additional energy inaccuracy due to a nearly free rotation of these groups and in order to decrease the computational problem size. Thus the majority of computational results presented here are based on modeling for the $[Tp^{Me}]^-$ ligand, i.e., tris(3-methylpyrazol-1-yl)-borate. Starting geometry of **1′** was taken from the crystal structure of **1** with added missing hydrogen atoms of the hydroxy ligands. Geometries of the neutral complexes as well as their reduced/oxidized forms were optimized independently. In addition, geometries of the modified structures obtained by a removal from **1′** the inner 3-methyl groups in pyrazolyl rings as well as by a substitution of the hydroxy by methoxy ligands were optimized.

It was already pointed out in the literature[20,21] that the molecular conformation can strongly influence the electron-transfer dynamics. Therefore, for the mixed-valence monoanion we have performed the scan versus N14−Mo1···Mo2−N24 dihedral angle (later called $D_1$), i.e., around the Mo···Mo axis, with a subsequent optimization of other geometric parameters. The scan was carried out starting at the equilibrium geometry ($D_1$ close to 90°) up to a synperiplanar or antiperiplanar orientation of the nitrosyl groups ($D_1 = 0°$ or 180°, respectively).

**DFT Calculations.** Calculations were performed using Gaussian 03 (E.01 version)[22] software within unrestricted scheme, with hybrid B3LYP[23] functional (widely applied in the mixed-valence studies) and LANL2DZ[24] basis set (denoted as B1) with an effective core potential on the molybdenum atoms. For B1 geometries, single-point calculations with the extended basis set of triple-ζ quality with polarization functions for all atoms, labeled def2-TZVPP[25] (denoted as B2), were performed for frequencies and energetic properties. A similar procedure (DFT geometry optimization with the basis of double-ζ type, followed by single-point calculations with extended basis set and/or methodology) has already been used in many successful studies on transition-metal systems.[26−28] To raise the credibility of the final results, we have reoptimized geometries for selected structures with the def2-TZVPP basis and found only minor differences in crucial structural parameters. Additionally, for selected properties the performance of nonhybrid OLYP[23b,29] and BP86[23a,30] potentials was tested for both basis sets. Contour plots of spin densities and molecular orbitals were prepared using Gabedit software.[31]

Gas-phase equilibrium geometries were used to estimate solvent effects by means of the polarized continuum model (PCM). The dielectric constant of the actual dichloromethane solvent ($\varepsilon = 8.93$) and the UFF scheme for cavity generation were used for the single-point computations. IR spectra were calculated for the equilibrium geometries for the gas-phase models, using a standard harmonic approximation.

Experimental one-electron redox potentials, $E_{1/2}$ (in V), are directly related to the total free energy of an electron attachment in solution $\Delta G^{EA}(sol)$ by the Nernst equation:

$$\Delta G^{EA}(sol) = -FE_{1/2}{}^{calc} \quad (1)$$

$\Delta G^{EA}(sol)$ has been calculated (at 298.15 K) from the difference of total energies of the oxidized and reduced forms, $E^{ox}(SCF)$ and $E^{red}(SCF)$, computed in the gas phase using a standard self-consistent field (SCF) procedure, according to the following equations:[32]

$$\Delta H^{EA}(SCF) = E^{ox}(SCF) - E^{red}(SCF) \quad (2)$$

$$\Delta H^{EA}(gas) = \Delta H^{EA}(SCF) + \Delta ZPE \quad (3)$$

$$\Delta G^{EA}(gas) = \Delta H^{EA}(gas) - T\Delta S(gas) \quad (4)$$

$$\Delta G^{EA}(sol) = \Delta G^{EA}(gas) + \Delta_s G \quad (5)$$

where $\Delta_s G$ is the free energy of solvation computed using PCM model, $\Delta H^{EA}(gas)$ is the electron attachment enthalpy in gas phase, and $\Delta S(gas)$ and $\Delta ZPE$ are the entropy and the zero point energy differences, respectively, between oxidized and reduced species in a gas phase obtained from vibrational analysis. The redox potential for ferrocene is referenced to a standard hydrogen electrode (SHE) with a specific absolute potential (4.43 eV);[33] this value was subtracted from the computed potential. All $E_{1/2}$ values for Mo complexes are reported versus $FeCp_2{}^{0/+}$.

**Single-Crystal X-ray Diffraction.** A red monocrystal of $\mathbf{1}\cdot 2C_6H_5CH_3$ was grown by slow evaporation of solvent from a concentrated toluene solution. The single-crystal diffraction

(21) Benniston, A. C.; Harriman, A. *Chem. Soc. Rev.* **2006**, *35*, 169.
(22) Frisch, M. J.; Trucks, G. W.; Schlegel, H. B.; Scuseria, G. E.; Robb, M. A.; Cheeseman, J. R.; Montgomery, J. A., Jr.; Vreven, T.; Kudin, K. N.; Burant, J. C.; Millam, J. M.; Iyengar, S. S.; Tomasi, J.; Barone, V.; Mennucci, B.; Cossi, M.; Scalmani, G.; Rega, N.; Petersson, G. A.; Nakatsuji, H.; Hada, M.; Ehara, M.; Toyota, K.; Fukuda, R.; Hasegawa, J.; Ishida, M.; Nakajima, T.; Honda, Y.; Kitao, O.; Nakai, H.; Klene, M.; Li, X.; Knox, J. E.; Hratchian, H. P.; Cross, J. B.; Bakken, V.; Adamo, C.; Jaramillo, J.; Gomperts, R.; Stratmann, R. E.; Yazyev, O.; Austin, A. J.; Cammi, R.; Pomelli, C.; Ochterski, J. W.; Ayala, P. Y.; Morokuma, K.; Voth, G. A.; Salvador, P.; Dannenberg, J. J.; Zakrzewski, V. G.; Dapprich, S.; Daniels, A. D.; Strain, M. C.; Farkas, O.; Malick, D. K.; Rabuck, A. D.; Raghavachari, K.; Foresman, J. B.; Ortiz, J. V.; Cui, Q.; Baboul, A. G.; Clifford, S.; Cioslowski, J.; Stefanov, B. B.; Liu, G.; Liashenko, A.; Piskorz, P.; Komaromi, I.; Martin, R. L.; Fox, D. J.; Keith, T.; Al-Laham, M. A.; Peng, C. Y.; Nanayakkara, A.; Challacombe, M.; Gill, P. M. W.; Johnson, B.; Chen, W.; Wong, M. W.; Gonzalez, C.; Pople, J. A. *Gaussian 03*, version E.01; Gaussian, Inc.: Wallingford, CT, 2004.
(23) (a) Becke, A. D. *Phys. Rev. A: At., Mol., Opt. Phys.* **1988**, *38*, 3098. (b) Lee, C.; Yang, W.; Parr, R. G. *Phys. Rev. B: Condens. Matter Mater. Phys.* **1988**, *37*, 785. (c) Becke, A. D. *J. Chem. Phys.* **1993**, *98*, 5648. (d) Becke, A. D. *J. Chem. Phys.* **1993**, *98*, 1372.
(24) Hay, P. J.; Wadt, W. R. *J. Chem. Phys.* **1985**, *82*, 299.
(25) Weigend, F.; Ahlrichs, R. *Phys. Chem. Chem. Phys.* **2005**, *7*, 3297.
(26) Shaik, S.; Cohen, S.; Wang, Y.; Chen, H.; Kumar, D.; Thiel, W. *Chem. Rev.* **2010**, *110*, 949.
(27) Popescu, D.-L.; Chanda, A.; Stadler, M.; de Oliveira, F. T.; Ryabov, A. D.; Munck, E.; Bominaar, E. L.; Collins, T. J. *Coord. Chem. Rev.* **2008**, *252*, 2050.
(28) Chen, H.; Song, J.; Lai, W.; Wu, W.; Shaik, S. *J. Chem. Theory Comput.* **2010**, *6*, 940.
(29) Handy, N. C.; Cohen, A. J. *Mol. Phys.* **2001**, *99*, 403.
(30) Perdew, J. P. *Phys. Rev. B: Condens. Matter Mater. Phys.* **1986**, *33*, 8822.
(31) Allouche, A. R. *Gabedit* ; http://gabedit.sourceforge.net/.
(32) Baik, M.-H.; Friesner, R. A. *J. Phys. Chem. A* **2002**, *106*, 7407 and references therein.
(33) Reiss, H.; Heller, A. *J. Phys. Chem.* **1985**, *89*, 4207.

**Table 1.** X-ray Crystallographic Data for $\mathbf{1}\cdot 2C_6H_5CH_3$

| | $\mathbf{1}\cdot 2C_6H_5CH_3$ |
|---|---|
| formula | $C_{44}H_{60}B_2Mo_2N_{14}O_5$ |
| fw | 1078.56 |
| crystal system | triclinic |
| space group | *P*-1 |
| *a*, Å | 12.282(5) |
| *b*, Å | 14.201(5) |
| *c*, Å | 15.448(5) |
| α, ° | 74.436(5) |
| *β*, ° | 79.060(5) |
| *γ*, ° | 81.929(5) |
| *V*, Å$^3$/Z | 2537.0(16)/2 |
| $\rho_{calcd}$, g cm$^{-3}$ | 1.412 |
| reflns collected/$2\Theta_{max}$ | 18 159/55 |
| unique reflns ($R_{int}$) | 11 461 (0.0503) |
| $R_1$ ($I > 2\sigma(I)$) | 0.0792 |
| $wR_2$ (all data) | 0.1725 |

data were collected on a Nonius Kappa CCD equipped with a Mo Kα (*λ* = 0.71073 Å) radiation source and a graphite monochromator, at 293 K. Positions of the nonhydrogen (non-H) atoms were determined by direct methods using SIR97.[34] Refinement and further calculations were carried out using SHELXL-97.[35] The non-H atoms, with exceptions of the disordered C atoms of toluene, were refined anisotropically using weighted full-matrix least-squares on $F^2$. All hydrogen atoms joined to carbon atoms of organic component of the discussed compound **1** were positioned with an idealized geometry and refined using a riding model with Uiso(H) fixed at 1.2 Ueq(C) for aromatic C−H and 1.5 Ueq(C) for the methyl groups. Hydrogens joined to boron atoms were found from the difference Fourier map. Unfortunately, the positions of the hydrogen atom of OH groups coordinated to molybdenum could not be determined. As mentioned above, one of the toluene molecules is strongly disordered. Any attempts of modeling this disorder and refining with partial occupancies of the atoms gave no satisfactory convergence. For this reason the carbon atoms of this molecule were refined with the isotropic displacement parameters. Furthermore, the distances and angles were restrained to ensure the proper geometry of this toluene molecule.

Selected crystallographic data for the studied compound are shown in Table 1 (see CIF file in the Supporting Information for details). The figure showing the molecular structure was prepared using ORTEP3 software.[36]

## Results and Discussion

**X-ray Single-Crystal and DFT-Optimized Structures of a Neutral Precursor.** The molecular structure of $\mathbf{1}\cdot 2C_6H_5CH_3$ is shown in Figure 1. The crystal has a layered structure with a solvating toluene placed between the layers formed by the molecules of the complex. The solvent is held by van der Waals forces, whereas the short $C^4_{(pz)}-O_{(NO)}$ distances (ca. 3.3 Å) between the molecules of the complex as well as the intramolecular $C_{(Me\text{-}pz)}-O_{(NO)}$ distances $C^4_{(pz)}-O_{(NO)}$ (ca. 3.2 Å) appear to be weak hydrogen bonds of the C−H···O type. Selected observed and computed (DFT-optimized structures in the gas phase) structural parameters are given in Table 2. The bimetallic core is based on the two distorted octahedral units in a near eclipsed array, while the relative configurations

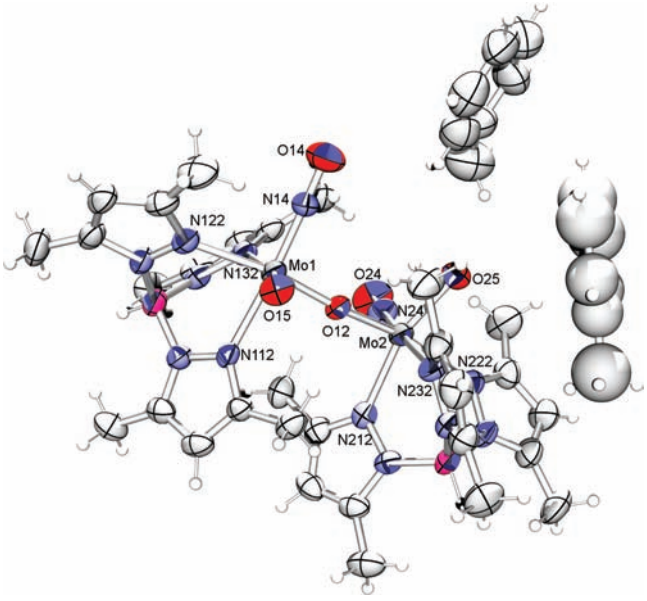


**Figure 1.** ORTEP drawing for the X-ray structure of $[\{Mo(NO)(Tp^{Me2})(OH)\}_2(\mu\text{-}O)]\cdot 2C_6H_5CH_3$ (**1**), showing the numbering scheme. Displacement ellipsoids are drawn at 50% probability level.

of Mo1 and Mo2 are *R* and *S*, respectively. The Mo−O−Mo bridge is slightly bent, and the ca. 6.4° of deviation from linearity resembles that of the diiodide analogue, with an average of 171.4(9)° for both of its enantiomers. This is due to a nonbonding repulsion caused by the methyl groups attached to the face-to-face pyrazolyl rings of the adjacent $[Tp^{Me2}]^-$ ligands, e.g., $C116_{(Me,pz)}-$N212 distance is 3.45 Å. The deviation from linearity of the Mo1−O12−Mo2 bridge is also reflected by the computed value of 171.0°. The calculations emphasize some bridge asymmetry, which is in accordance with the spectral results (nonequivalence of the Mo centers is manifested in the occurrence of the two $\nu_{NO}$ frequencies as well as in the NMR spectra). The relatively short $Mo-O_{bridge/hydroxy}$ bond distances (in the range of 1.897(4)−1.946(5) Å) indicate a conspicuous $d\pi_{Mo}-p\pi_O$ interaction, confirmed by the calculations (vide infra) and are a consequence of the electron deficiency of 16*e* metal centers. In comparison, in the case of a pure $Mo^{II}-O$ *σ* bond, a distance of ca. 2.11 Å is expected.[37] The observed Mo···Mo distance equals 3.788(2) Å and is well predicted by the DFT (ca. 3.82 Å). The most essential feature of this structure is that the nearly linear nitrosyls (Mo−N−O angle equal to 178.3(5) and 176.7(5)°) lie along nearly orthogonal directions. Such an arrangement is identical to that adopted by the structurally characterized complexes $[X(Tp^{Me2})(ON)MoOMo(NO)(Tp^{Me2})Y]$ (two enantiomers of the same species, where X = Y = I and an asymmetrically substituted compound where X = I and Y = NHMe)[7,8] and is satisfactorily modeled, i.e., dihedral angles N14−Mo1···Mo2−N24 ($D_1$) are 85.4(27) (measured) and 90.8° (calculated).

**Vibrational Analysis.** Selected stretching vibrations of complex **1** and its mimic **1′**, including the reduced/oxidized forms, are shown in Table 3. The IR spectra of the neutral complexes exhibit two $\nu_{NO}$ frequencies, which are very well modeled. The calculated asymmetric $\nu_{MoOMo}$

(34) Altomare, A.; Burla, M. C.; Camalli, M.; Cascarano, G. L.; Giacovazzo, C.; Guagliardi, A.; Moliterni, A. G. G.; Polidori, G.; Spagna, R. *J. Appl. Crystallogr.* **1999**, *32*, 115.

(35) Sheldrick, G. M. *SHELXS-97*, release 97-2; University of Göttingen: Göttingen, Germany, 1998.

(36) Farrugia, L. J. *J. Appl. Crystallogr.* **1997**, *30*, 565.

(37) Cotton, F. A.; Norman, J. G. *J. Am. Chem. Soc.* **1972**, *94*, 5697.

**Table 2.** Selected Structural Parameters for Complexes **1** and **1′** Including Reduced/Oxidized Forms

| parameter | **1** (obs.) | **1′** (calcd) | **1′**$^{-}$ (calcd) | **1′**$^{+}$ (calcd) |
|---|---|---|---|---|
| | | Distances (Å) | | |
| Mo1−O12 | 1.897(4) | 1.915 | 2.074 | 2.053 |
| Mo1−N14 | 1.764(5) | 1.786 | 1.782 | 1.793 |
| Mo1−O15 | 1.951(4) | 1.972 | 2.058 | 1.947 |
| N14−O14 | 1.205(7) | 1.236 | 1.260 | 1.222 |
| Mo2−O12 | 1.897(4) | 1.922 | 1.852 | 1.827 |
| Mo2−N24 | 1.742(5) | 1.785 | 1.778 | 1.864 |
| Mo2−O25 | 1.945(5) | 1.982 | 2.015 | 1.962 |
| N24−O24 | 1.208(7) | 1.233 | 1.251 | 1.213 |
| Mo···Mo | 3.788(2) | 3.825 | 3.873 | 3.869 |
| | | Angles (°) | | |
| O12−Mo1−N14 | 96.5(2) | 97.9 | 98.3 | 94.1 |
| O12−Mo1−O15 | 105.38(18) | 102.0 | 94.1 | 97.8 |
| Mo1−N14−O14 | 178.4(5) | 176.2 | 174.9 | 178.8 |
| O12−Mo2−N24 | 98.1(2) | 96.0 | 102.0 | 96.4 |
| O12−Mo2−O25 | 103.65(19) | 105.3 | 105.7 | 105.9 |
| Mo2−N24−O24 | 176.7(5) | 177.7 | 176.9 | 174.7 |
| Mo1−O12−Mo2 | 173.6(2) | 171.0 | 161.1 | 171.5 |
| | | Torsion Angles (°) | | |
| N14−Mo1···Mo2−N24 ($D_1$) | 85.36(27) | 90.8 | 98.9 | 92.0 |
| N14−Mo1−O12-Mo2 ($D_2$) | −43(2) | −59.3 | −82.3 | −67.8 |
| N24−Mo2−O12-Mo1 ($D_3$) | −43(2) | −32.1 | −18.3 | −24.5 |

**Table 3.** Selected Vibrational Frequencies (cm$^{-1}$) of Complex **1** and Its Model **1′** Including the Reduced/Oxidized Species

| complex | $\nu_{NO}$ | $\nu_{MoOMo}$ |
|---|---|---|
| **1** (obs.)[a] | 1628, 1653 | 777 |
| **1′** (calcd)[b] | 1624, 1646 | 803 |
| **1′**$^{-}$ (calcd)[b] | 1527, 1584 | 796 |
| **1′**$^{+}$ (calcd)[b] | 1664, 1678 | 788, 827 |

[a] Measured in solid (KBr); data from ref 8. [b] Obtained with the B3LYP functional (B1 basis).

mode and the remaining absorptions attributable to the [Tp$^{Me}$]$^{-}$ ligand (particularly the pulsating mode of the pyrazolyl rings $\nu_{C=C}$ at ca. 1540 cm$^{-1}$ and $\nu_{BH}$ at ca. 2589 cm$^{-1}$) are in agreement with the experimental data, whereas the position of $\nu_{OH}$ is substantially overshot. Upon reduction, both $\nu_{NO}$ bands in the computed spectrum are shifted toward red, and the splitting is wider relative to the neutral species ($\Delta\nu_{NO}$ rises from 25 to 57 cm$^{-1}$) which is consistent with a valence trapping in **1′**$^{-}$ on the infrared time-scale. This result could be compared to the experimentally analyzed [{Mo(NO)(Tp$^{Me2}$)Cl}$_2$($\mu$-O)]$^{-}$, which behaves similarly.[7] Torsional vibrations appear in the 50−200 cm$^{-1}$ region, attributable to the rotation around the Mo···Mo axis which changes the relative orientation of the {MoNO} groups. One-electron oxidation of **1′** generates a monocation with two hypsochromically shifted $\nu_{NO}$ frequencies. Both hybrid and nonhybrid (BP86 and OLYP) functionals yield reasonable results, although the $\nu_{NO}$ vibrations fall below experimental values.

**Redox Potentials.** One-electron redox potentials relative to the ferrocene for complex **1** and its mimic **1′**, as defined by Scheme 1, are presented in Table 4. Voltammetrically established potentials, $E^1_{1/2}$ and $E^3_{1/2}$, of the formation of {17*e*:16*e*}$^{-}$ and {16*e*:15*e*}$^{+}$ mixed-valence

**Table 4.** One-Electron (in V, vs $FeCp_2^{0/+}$) Redox Potentials for Complex **1** and its Mimic **1′** in $CH_2Cl_2$

| | **1** (obs.)[a] | **1′** (calcd)[b] |
|---|---|---|
| | Reduction | |
| $E^1_{1/2}$ | −1.77 | −1.73 |
| $E^2_{1/2}$ | [c] | −2.67 |
| $\Delta_{red}E_{1/2}$ | (>0.89)[d] | 0.94 |
| | Oxidation | |
| $E^3_{1/2}$ | +0.60[e] | +0.79 |
| $E^4_{1/2}$ | [c] | +1.84 |
| $\Delta_{ox}E_{1/2}$ | | 1.05 |

[a] Data taken from ref 8. [b] Obtained from the B3LYP:UFF calculations (B2 basis). [c] Not observed because the reduction or oxidation waves occur at potentials beyond the decomposition potentials of the solvent. [d] Estimated since the reduction wave of $CH_2Cl_2$ appears at ca. −2.66 V versus $FeCp_2^{0/+}$. [e] Anodic peak, chemically irreversible.

**Scheme 1.** One Electron-Transfer Chain for the Series **1**/**1′**$^{z}$ ($z$ = 2−,1−, 0, 1+, and 2+)

$$\{15e{:}15e\}^{2+} \overset{-e}{\underset{E^4_{1/2}}{\rightleftharpoons}} \{16e{:}15e\}^{+} \overset{-e}{\underset{E^3_{1/2}}{\rightleftharpoons}} \mathbf{\{16e{:}16e\}} \overset{+e}{\underset{E^1_{1/2}}{\rightleftharpoons}} \{17e{:}16e\}^{-} \overset{+e}{\underset{E^2_{1/2}}{\rightleftharpoons}} \{17e{:}17e\}^{2-}$$

species, respectively, are best reproduced by the B3LYP:UFF (B2 basis) calculations; however, the first oxidation potential is slightly overestimated, which is a known tendency of the DFT/B3LYP calculations.[38] A calculated separation between the first and second ($E^1_{1/2}$ and $E^2_{1/2}$) reduction potentials ($\Delta_{red}E_{1/2}$ = 0.94 V) closely resembles the estimated value for **1** (see footnote *c* in Table 4) as well as the exact value measured for [{Mo(NO)(Tp$^{Me2}$)I}$_2$($\mu$-O)] ($\Delta_{red}E_{1/2}$ = 0.99 mV in $CH_2Cl_2$)[7] and further confirms very strong metal−metal interactions. In contrast to rather accurate B3LYP results, both BP86 and OLYP functionals overestimate the reduction potentials, nevertheless, the redox potential splitting is accurately reproduced. The computed electrochemical interactions in the oxidized complex **1′**, measured by $\Delta_{ox}E_{1/2} = E^4_{1/2} - E^3_{1/2}$ are also close to 1000 mV. The large splitting between the single-electron reduction as well as oxidation processes goes in line with the high thermodynamic stability of the mixed-valence ions relative to their isovalent forms[39] and results from the through-space Coulombic effects in the fully localized states (see the paragraphs below and the calculated distribution of spin density in Figure 5).

**Analysis of Geometrical and Electronic Structure of Reduced/Oxidized Species.** The influence of the conformation of two-center radicals linked by the bridge on a prospective electron delocalization was recently reported in literature.[20,21,40,41] The authors have already pointed out in refs 40 and 41 that the angle between the plane of the bridging ligand and the equatorial plane of the metal

(38) Roy, L. E.; Jakubikova, E.; Guthrie, M. G.; Batista, E. R. *J. Phys. Chem. A* **2009**, *113*, 6745.
(39) Mixed-valence ions stability is expressed by large value of the comproportionation constant, $K_c$, greater than $10^{15}$. It is calculated from $K_c = e^{F\Delta E^{\circ}/(RT)}$ (at 298 K; equality of $E^{\circ}$ and $E_{1/2}$ were assumed).
(40) Benniston, A. C.; Harriman, A.; Li, P.; Sams, C. A.; Ward, M. D. *J. Am. Chem. Soc.* **2004**, *126*, 13630.
(41) Adams, H.; Costa, P. J.; Newell, M.; Vickers, S. J.; Ward, M. D.; Félix, V.; Thomas, J. A. *Inorg. Chem.* **2008**, *47*, 11633.

**Scheme 2.** Angles Definition for (a) Large and (b) Small Angles ∠N14−Mo1···Mo2−N24[a]

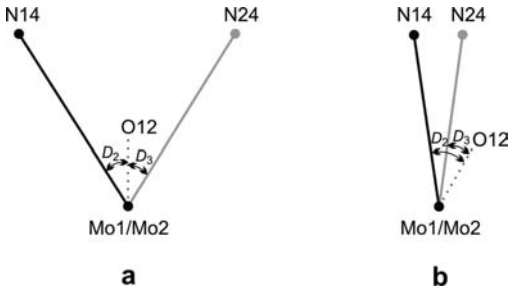


[a] View along Mo···Mo axis; $D_2$ = ∠N14−Mo1−O12−Mo2 and $D_3$ = ∠N24−Mo2−O12−Mo1.

coordination spheres was the important factor influencing the electron transfer in the mixed-valence $Ru^{III/II}$-based Creutz−Taube analogues. In our study, the two equatorial planes are defined by the position of the NO ligand, assumed along the $z$ axis in each center, and are nearly perpendicular in the lowest energy conformation. Therefore, we were prompted to perform a geometry scan with respect to the relative orientation of the two $\{Mo(NO)\}^{2+,3+}$ cores for the singly reduced **1′**. Hereto the scan versus N14−Mo1···Mo2−N24 dihedral angle ($D_1$) was performed with a subsequent optimization of the other geometry parameters. One of the key factors relating to the overall conductivity of the bridge is the proper matching of the molecular orbitals on the adjacent subunits to form a continuous medium.[21,42] Therefore, the position of the oxygen bridge should be analyzed together with the relative orientation of the two nitrosyls. Indeed, the bridge becomes bent for a range of $D_1$ angles, and its position was found to be the important geometrical parameter coupled to the scanned dihedral angle. It was monitored via two angular distances (absolute values of $D_2$ and $D_3$) between the Mo1−$O_{bridge}$−Mo2 plane and the N14−Mo1···Mo2 or N24−Mo2···Mo1 planes, respectively, measuring the bridge position with respect to the two local $z$ axes set by the direction of each Mo−NO moiety (see Scheme 2).

Table 5 and Figures 2 and 3 illustrate the results of the analysis. Figure 2 shows the dependence of total energy on the scanned dihedral angle $D_1$, while Figure 3 describes the degree of the electron delocalization along the scan, as measured by the spin density population on the Mo2 center (not reduced). The absolute values of $D_2$ and $D_3$ angles for critical structures along the scan versus $D_1$ are listed in Table 5, together with other important geometrical parameters. It follows from Figure 2 that the bimetallic radical $\mathbf{1'}^{-}$ becomes strongly energetically disfavored (by ca. 16 kcal/mol) for syn or anti arrangement of the nitrosyl groups ($D_1$ angle near 0° or 180°). The large torsional deflection is a feature of both isovalent and mixed-valent bimetallic complexes containing $\{Mo(NO)\}^{2+,3+,or\ 4+}$ cores ($\mathbf{1'}^{-1,0,+1}$). The optimal geometries of the two modified structures, containing either the nonsubstituted Tp or the species with substituted OH ligands, also displayed strongly twisted nitrosyls (ON···NO angle in a range 84.7−100°). This shows that releasing the steric constraints due to the repulsion of Tp−methyl groups does not influence the perpendicular conformation of the NO groups.[43] Hydrogen bonds are formed during the scan along the $D_1$ angle: OH···ON at $D_1$ ca. 110° or OH···OH at $D_1$ ca. 5°. The former stabilizes the twisted conformation, whereas the latter is too weak to stabilize the syn conformation. The X-ray study of the related $[\{Mo^{V}(O)TpCl\}_2(\mu\text{-}O)]$ complex,[44] isolated as two geometrical isomers ($C_2$ and $C_i$), showed that this species has terminal oxo ligands lying in the same plane or in slightly twisted (dihedral angle 13.5°), with linear or almost linear (177.3°) Mo−O−Mo bridge arrangement. The $[\{Mo(O)(Tp^{Me2})Cl\}_2(\mu\text{-}O)]$ complex has a structure of a similar type, i.e., the oxo groups in the $C_2$-related $\{Mo(O)(Tp^{Me2})Cl\}$ units are anti.[45] Unfortunately, there is no information about the properties of the mixed-valent forms, but most probably, the one-electron oxidation will not involve any essential change in their geometries, favoring the electron transfer in both cases.

These sharply distinct conformational properties of the $\mu$-oxo complexes with either $\{Mo(NO)\}^{3+,2+}$ or $\{Mo(O)\}^{4+,3+}$ cores may be rationalized by the inspection of their electronic structures following from a qualitative orbital diagram depicted in Scheme 3. The two highest doubly occupied orbitals are composed of the two $d_{xz}$ metal orbitals (with $z$ axis pointing along each Mo−NO and $x$ axis along the Mo···Mo direction). In contrast, these orbitals are empty in the case of the $Mo^{V}/Mo^{VI}$ pair with oxo ligands. The two in-plane electron pairs should markedly contribute to repulsive interaction destabilizing the molecule in either syn or anti conformation (Scheme 4). As a result, the conformation with nearly orthogonal nitrosyls, where the two $d_{xz}$ electron pairs avoid each other most effectively, becomes the minimum energy structure for **1′**. The opposite energetic contribution could be brought by the tendency to through-bond delocalization of the unpaired electron, due to the interaction of the singly occupied $d_{xy}$ orbital of Mo1 with the empty $d_{xy}$ orbital on Mo2, possibly mediated by the bridging oxygen $p_y$ orbital. This stabilizing interaction would be maximal for coplanarity of two $d_{xy}$ and oxygen $p_y$ orbitals, i.e., for an in-plane arrangement of NO ligands and the bridge. However, a destabilizing repulsion between $d_{xz}$ electron pairs, coplanar with the occupied $p_{zO}$, clearly prevails in our case, and thus complex **1′** shows a torsionally distorted minimum energy structure, minimizing the repulsion but blocking the electron flow channel.

For ON···NO twist angles close to 90° (minimum energy conformation), the bridging oxygen lays in between the N14−Mo1···Mo2 and N14−Mo2···Mo1 planes. The $D_2$ and $D_3$ angles (defined in Scheme 2) yield additional information about the prospective mixing between the $p_O$ and $d_{Mo}$ orbitals on either center; $p_{z,O}$ is

(42) Benniston, A. C.; Harriman, A.; Li, P.; Sams, C. A. *Phys. Chem. Chem. Phys.* **2004**, *6*, 875.

(43) Strongly twisted geometry has also been found for other structurally characterized {(ON)MoOMo(NO)} complexes containing non-Tp ligands, e.g., $[\{Mo^{II}(NO)('S_4')\}_2(\mu\text{-}O)]$ ('$S_4$' is 2,3,8,9-dibenzo-1,4,7,10-tetrathiadecane-(2-); (see Sellmann, D.; Seubert, B.; Knoch, F.; Moll, M. *Z. Anorg. Allg. Chem.* **1991**, *600*, 95) or the 16e $[Cp^*Mo(NO)R]_2(\mu\text{-}O)$ complexes ($Cp^*$ is $\eta^5$-$C_5Me_5$, R is $CH_2SiMe_3$ or Me; see Legzdins, P.; Lundmark, P. J.; Phillips, E. C.; Rettig, S. J.; Veltheer, J. E. *Organometallics* **1992**, *11*, 2991 and Sharp, W. B.; Daff, P. J.; McNeil, W. S.; Legzdins, P. *J. Am. Chem. Soc.* **2001**, *123*, 6272).

(44) Lincoln, S.; Koch, S. A. *Inorg. Chem.* **1986**, *25*, 1594.

(45) Millar, A. J.; Doonan, C. J.; Laughlin, L. J.; Tiekink, E. R. T.; Young, C. G. *Inorg. Chim. Acta* **2002**, *337*, 393.

**Table 5.** Important Geometrical Parameters for Characteristic ON···NO Arrangements in the Structure of $\mathbf{1}'^{-}$

| ON···NO arrangement | $D_1$ (°) | $D_2$ (°) | $D_3$ (°) | Mo1−O−Mo2 (°) | Mo1···Mo2 (Å) | $\Delta E$ (kcal mol$^{-1}$) |
|---|---|---|---|---|---|---|
| syn | 0 | 50.4 | 51.8 | 138.4 | 3.73 | +16.8 |
| maximum delocalization | 23 | 41.1 | 17.8 | 147.7 | 3.78 | +16.5 |
| minimum energy | 98.9 | 82.3 | 18.3 | 161.1 | 3.87 | 0 |
| anti | 178 | 135.0 | 47.0 | 176.2 | 3.97 | +17.0 |

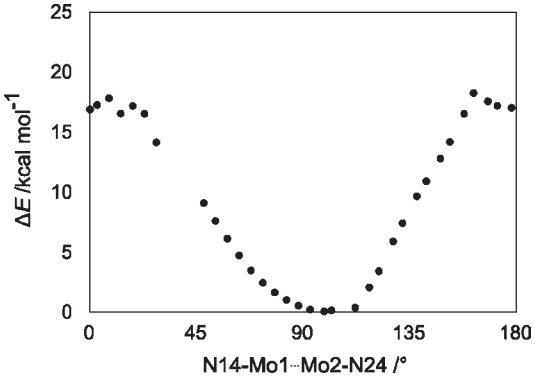


**Figure 2.** Total energy variation along the scan vs $D_1$ dihedral angle in $\mathbf{1}'^{-}$.

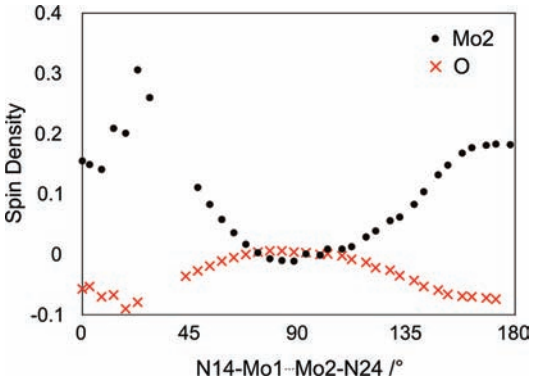


**Figure 3.** Spin density on Mo2 (not reduced) and on bridging oxygen vs $D_1$ dihedral angle in $\mathbf{1}'^{-}$.

nearly coplanar with the $d_{xz}$ orbital on Mo1 in the geometry of reduced or oxidized $\mathbf{1}'$. The filled−filled interaction between the $d_{xz,Mo1}$ and $p_{z,O}$ orbitals is repulsive and depends on the $D_2$ angle; it increases with $D_2$ approaching 90°. The $D_3$ angle adds roughly to 90°, thus the other Mo avoids this type of repulsion. Indeed, the Mo1−O12 and Mo2−O12 distances calculated for the minimum energy structure of singly reduced (oxidized) complex $\mathbf{1}'$ are 2.074 (2.053) and 1.852 (1.827) Å, respectively. For an anti arrangement of the nitrosyls, the bridge is nearly linear, and its angular position looses meaning. Here, as well repulsive interactions as density delocalization via hole transfer mechanism would be possible between Mo centers. Therefore, the structure is energetically destabilized, while electron delocalization is triggered (see Figure 3). However, due to bridge straightening the distance between the metal centers is large, which reduces as well the favorable as unfavorable electronic interactions.

For $D_1$ angles smaller than 60°, the picture is different. There is a steric hindrance for the bridging oxygen in the space between $\{Mo(NO)\}^{2+,3+}$ cores; the bridge becomes more bent and is pushed outside the two planes (see Scheme 2). For a parallel arrangement of the two nitrosyls,

**Scheme 3.** Qualitative Orbital Diagram for $\{MoNO\}^{2+,3+}$ Cores Linked by $\mu$-oxo Bridge

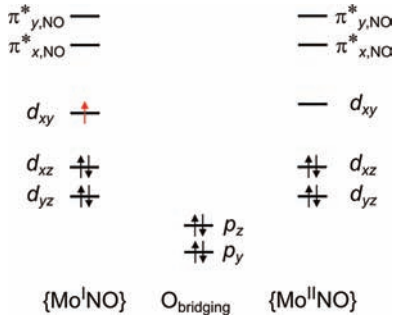


**Scheme 4.** (a) Schematic Representation of the Repulsion Between Mo $d_{xz}$ Electron Pairs[a] and (b) in Complexes Containing $\{MoO\}^{3+,4+}$ Cores[b]

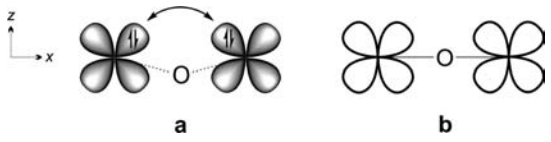


[a] Likely for $\mu$-oxo complexes with $\{MoNO\}^{2+,3+}$ cores in syn or anti NO orientation. [b] This is not expected since $d_{xz}$ orbitals are empty.

the oxygen bridge is bent by 138.4° and pushed away by ca. 50° from both local $xy$ planes, which reduces both the repulsive electronic interaction and electron delocalization (see Figures 2 and 3). Maximum degree of electron delocalization is found for $D_1$ angle equal to 23°. For this conformation the angular mismatch between O $p_y$ and both $d_{xy}$ local planes is reduced, which enables the electron delocalization via a hole-transfer mechanism and offers a compromise between the favorable electron delocalization and a destabilizing repulsion. Figure 3 nicely illustrates the dependence of the electron density delocalization on the relative configurations of the two metal centers and the bridge. Near the energy minimum no spin density is observed on either the Mo2 center or the bridging oxygen. For structures showing a noticeable electron transfer, the bridge clearly participates in this process, transferring the spin density to Mo2 and acquiring some spin density back from Mo1. For syn nitrosyl orientation the density flow is reduced with respect to the maximum (by a bridge distortion), whereas for an anti arrangement the Mo···Mo distance is significantly increased (by ca. 0.25 Å, see Table 5), which also reduces the orbital overlap and the electron delocalization.

In order to further illustrate the electronic interactions in the studied complexes, qualitative diagrams of the important Kohn−Sham molecular orbitals are presented for the minimum energy structure (Figure 4a) and for the maximum delocalization structure (Figure 4b). Orbital contours are drawn for the majority spin orbitals with a dominant contribution from Mo 4d functions. The diagrams fully support

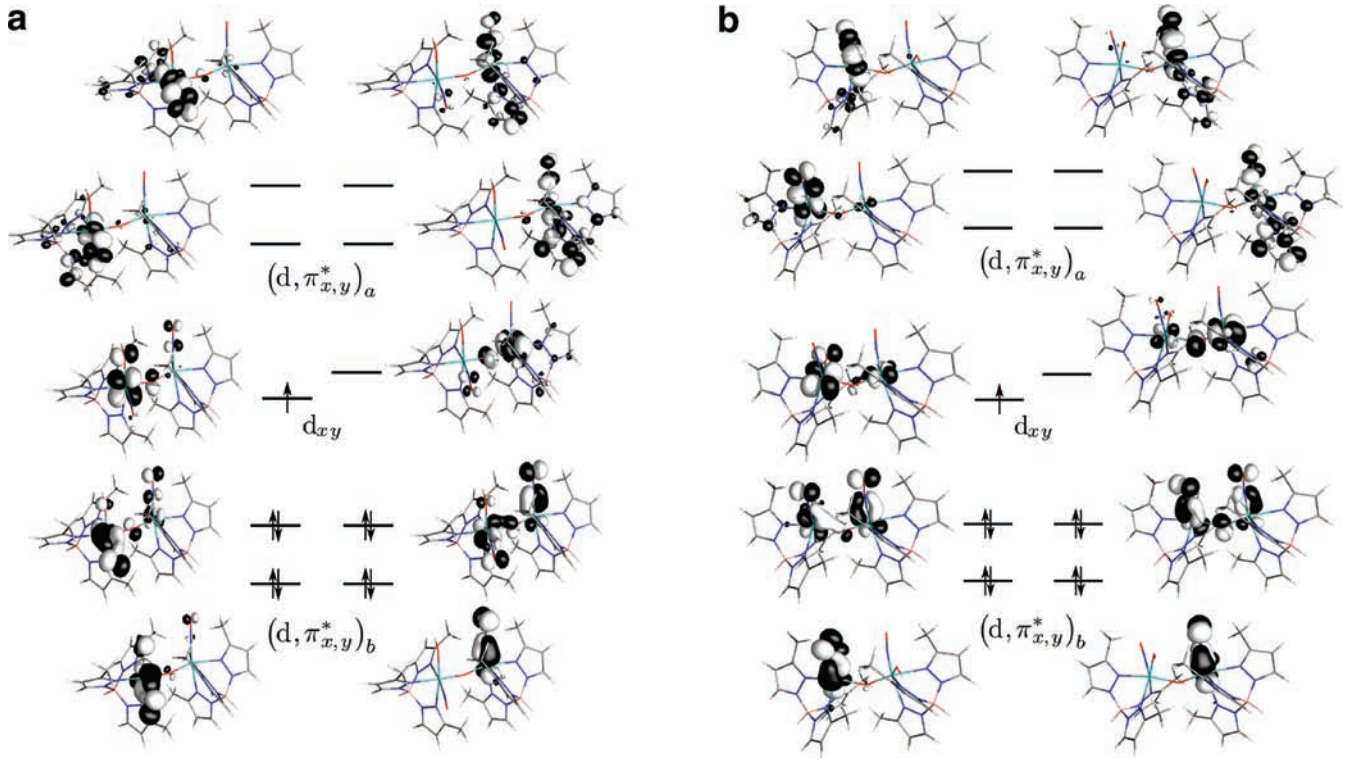


**Figure 4.** (a) Calculated important molecular orbitals diagram for optimal geometry ($D_1$ = 98.9°) of complex $\mathbf{1'}^-$. Contour plots for isovalue 0.05. (b) Calculated important molecular orbitals diagram for a maximum electron delocalization geometry of complex $\mathbf{1'}^-$ ($D_1$ = 23°). Contour plots for isovalue 0.05.

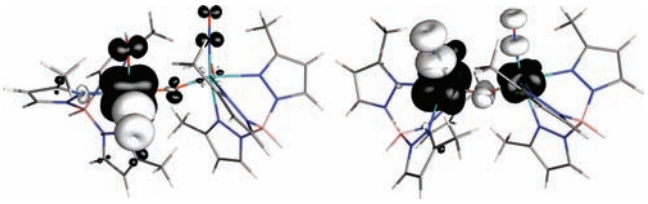

**Figure 5.** Calculated spin density profiles for optimal (left, $D_1$ = 98.9°) and maximum electron delocalization (right, $D_1$ = 23°) geometry of complex $\mathbf{1'}^-$. Contour plots for isovalue 0.002.

the tentative interpretation of the electronic and geometrical structure of $\mathbf{1'}^-$ based on Schemes 3 and 4. Two pairs of highest doubly occupied orbitals are composed of $d_{xz}$ and $d_{yz}$ Mo orbitals mixed with $\pi^*$ orbitals on NO (due to a strong covalent bonding), while the singly occupied molecular orbital is a $d_{xy}$ orbital. In the minimum energy structure the pairs of occupied $d_{xz}$ or $d_{yz}$ orbitals on the two Mo centers are in orthogonal planes, thus the repulsion between two electron densities is minimized. The two $d_{xy}$ orbitals are also mutually orthogonal and do not mix; the singly occupied molecular orbital is centered on Mo1 with no contribution from Mo2. Each of the metal $d_{xy}$ orbitals overlaps with the other p orbital on oxygen, therefore the hole-transfer mechanism cannot operate. On the contrary, in the structure showing the maximum electron delocalization ($D_1$ = 23°), corresponding pairs of Mo d orbitals are close to parallel. Therefore, here the $d_{xy}$ orbitals on two Mo centers may interact by mediation of the bridge which triggers the electron delocalization; however, the repulsion between the electron pairs in $d_{xz}$ orbitals is also large, raising the energy of this structure.

Table 6 and Figure 5 present the information on the dependence of the calculated spin density distribution on

**Table 6.** Spin Densities on Selected Atoms or Fragments in Complex $\mathbf{1'}^-$ for Selected Rotamers

| structure | Mo1 | $NO^{(1)}$ | $O_b$ | Mo2 | $NO^{(2)}$ |
|---|---|---|---|---|---|
| minimum energy | 1.21 | −0.38 | 0.00 | 0.00 | 0.05 |
| maximum delocalization | 1.09 | −0.36 | −0.09 | 0.31 | −0.10 |

the relative orientation of the two monomers in complex $\mathbf{1'}^-$. The spin density plot obtained for the minimum energy geometry of $\mathbf{1'}^-$ species is shown in the left panel of Figure 5. The localization of an additional unpaired electron on one Mo center is clearly visible. On the contrary, the analogous plot given for a structure with maximum electron delocalization, in the right panel of Figure 5, shows a conspicuous spin density on the second Mo center. A noticeable spin density on the bridging oxygen evidences the role of $2p_O$ in electron density delocalization. The oxygen carries a minority (spin-down) density; however, one should be aware that the magnitude of spin polarization may be overestimated due to correlation effects and the use of a hybrid (B3LYP) functional.[46] The natural spin orbital with 1.0 occupancy shown in Figure 6 is obviously free from spin polarization and should better correspond to actual density of the unpaired electron. It shows that although the spin density is strongly localized on Mo1 center, it is also significantly delocalized toward the second Mo for this structure. A similar reasoning may be carried in the case of one-electron oxidation. The contour of the natural spin orbital with 1.0 occupancy for $\mathbf{1'}^+$ in minimum energy geometry (Figure 7) indicates that the resulting spin density is localized on Mo2 center which suggests that the oxidation also leads to

(46) Radoń, M.; Broclawik, E.; Pierloot, K. *J. Phys. Chem. B* **2010**, *114*, 1518.

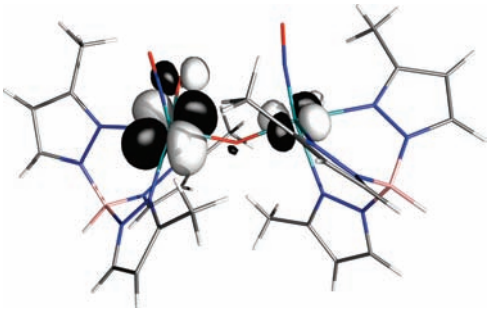

**Figure 6.** Plot of natural spin orbital with 1.0 occupation number for $\mathbf{1'}^{-}$ with $D_1 = 23°$ (maximum delocalization). Contour plot for isovalue 0.05.

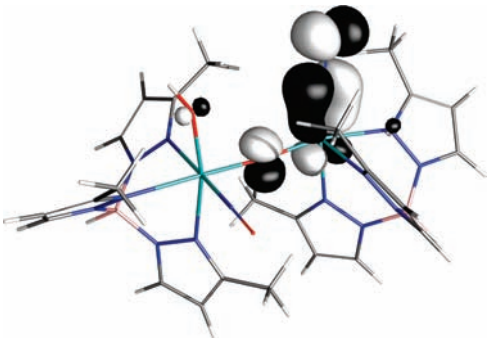

**Figure 7.** Plot of natural spin orbital with 1.0 occupation number for $\mathbf{1'}^{+}$ in an optimal geometry. Contour plot for isovalue 0.05.

the Class I mixed-valence $\{16e{:}15e\}^{+}$ complex $\mathbf{1'}^{+}$. Spatial distribution of an electron hole created by oxidation points at electron depletion from the Mo−NO strongly bonding region; therefore, significant elongation of the Mo2−N24 bond upon electron extraction should be expected, which is well reflected by calculated geometrical parameters (Table 2). This density depletion has apparently only minor influence on torsional distortion of the oxidized complex induced by $d_{Mo1}-d_{Mo2}$ filled−filled repulsion. Upon second oxidation or reduction, the two Mo centers become electronically equivalent, conserving the large torsional deflection ($D_1$ angles are 85.2 and 92.5°, respectively). The $\{17e{:}17e\}^{2-}$ biradical, corresponding to the double reduction process, has closely lying triplet and singlet states which corroborates the notion of weak magnetic coupling (negligible exchange coupling constant $J$) between the two Mo centers in the complex with strongly twisted geometry.

## Conclusions

The purpose of this work was to employ the density functional theory (DFT) modeling to examine the electronic communication in strongly interacting oxo-bridged dimolybdenum nitrosyl scorpionates having fully localized valences despite short (ca. 3.8 Å) Mo···Mo distance. Calculated (B3LYP) structural, electrochemical, and vibrational properties of the mimetic model $\mathbf{1'}$ are successfully related to the X-ray data, the voltammetrically established potentials of formation of both $\{17e{:}16e\}^{-}$ and $\{16e{:}15e\}^{+}$ mixed-valence species, and the IR spectra (particularly $\nu_{NO}$ frequencies) of **1**. The favorable, strongly twisted geometry, determined for **1** by X-ray diffraction and confirmed by DFT calculations for $\mathbf{1'}$ in this study, is a common feature of species belonging to this class of compounds and is shown here to fully block the channel for electron flow in the mixed-valence states. Therefore, our main goal was to resolve this still not fully understood puzzle: (i) how does a relative orientation of $\{Mo(NO)\}^{2+/3+}$ groups control the intramolecular electron transfer, and (ii) why, in the optimal geometry, the two NO ligands are mutually orthogonal.

To this end we have performed the scan along the prospective torsional degree of freedom with respect to the Mo···Mo axis, controlling the relative conformation of the two $\{Mo(NO)\}^{2+/3+}$ cores. Our results indicate that the favorable, strongly twisted geometry and putative rotational freedom of the bridging unit in $\mathbf{1'}$ or its one-electron reduced/oxidized forms is determined by the electronic structure, namely by the balance between destabilizing repulsion of the Mo-based (d, $\pi_x^*)_b$ electron pairs versus a favorable but relatively weak electron delocalization. The steric hindrance (nonbonding repulsion of the adjacent $Tp^x$ ligands and weak hydrogen-bonding interactions, i.e., OH···ON, OH···OH, and C−H···$O_{(NO/OH)}$) are shown to be of minor importance as neither the removal of the inner 3-Me groups of $[Tp^{Me}]^{-}$ ligands nor the substitution of the OH groups by $OCH_3$ ligands did substantially influence the minimum energy structure despite seemingly enabling higher rotational freedom. The $d_{xz}$ orbitals, responsible for enhanced electronic repulsion, are empty in the case of $[\{Mo^{V}(O)Tp^{x}Cl\}_2(\mu\text{-}O)]$ complexes, closely related to the studied species but having a syn or anti arrangement. Maximum delocalization of the unpaired electron in $\mathbf{1'}^{-}$ (measured as spin population on the Mo2 center) is achieved at a torsional deflection ((O)N−Mo1···Mo2−N(O) angle) equal to 23° at a cost of 16.5 kcal/mol. One-electron oxidation of $\mathbf{1'}$ generates a $\{16e{:}15e\}^{+}$ ion which is also entirely valence-trapped. A second reduction or oxidation produces the two equivalent Mo centers; the $\{17e{:}17e\}^{2-}$ biradical has closely lying triplet and singlet states, with potentially interesting magnetic properties (subject of further studies).

This work shows that the electron exchange along the Mo−O−Mo array in the originally fully valence-trapped (Class I) $\{17e{:}16e\}^{-}$ complexes could be torsionally induced (i.e., thermally activated in a high-boiling solvent or by the irradiation at ca. 50−200 $cm^{-1}$) which supports the postulated hypothesis[7,8] that the temperature dependence of the electron paramagnetic resonance (EPR) spectra of the related dibenzoate or dichloride $[\{Mo(NO)(Tp^{Me2})X\}_2(\mu\text{-}O)]^{-}$ (X = OCOPh or Cl) result from the electron-exchange behavior. Finally, the properties of the redox-active {(ON)MoOMo(NO)} complexes studied here might be relevant to the researchers concerned with design of prospective functional molecular materials; the very high stability of these complexes and easy substitution on the Mo center opens a way to construction of oligonuclear arrays based on the {(ON)MoOMo(NO)} unit.

**Acknowledgment.** The computations were performed at the Academic Computer Centre CYFRONET AGH (grants no. MNiSW/SGI4700/UJ/056/2007, MNiSW/IBM_BC_HS21/UJ/056/2007 and the PL-Grid project: POIG.02.03.00-00-007/08-00).

**Supporting Information Available:** Cartesian coordinates, IR spectra and redox-potentials for the computed structures (PDF file), and X-ray crystallographic data for **1** (CIF file). This material is available free of charge via the Internet at http://pubs.acs.org.